Surface Chemistry

DOI: 10.1002/anie.201402374

Crystal-Plane-Controlled Selectivity of Cu_2O Catalysts in Propylene Oxidation with Molecular Oxygen**

*Qing Hua, Tian Cao, Xiang-Kui Gu, Jiqing Lu, Zhiquan Jiang, Xiaorong Pan, Liangfeng Luo, Wei-Xue Li, and Weixin Huang**

Abstract: *The selective oxidation of propylene with O_2 to propylene oxide and acrolein is of great interest and importance. We report the crystal-plane-controlled selectivity of uniform capping-ligand-free Cu_2O octahedra, cubes, and rhombic dodecahedra in catalyzing propylene oxidation with O_2: Cu_2O octahedra exposing {111} crystal planes are most selective for acrolein; Cu_2O cubes exposing {100} crystal planes are most selective for CO_2; Cu_2O rhombic dodecahedra exposing {110} crystal planes are most selective for propylene oxide. One-coordinated Cu on $Cu_2O(111)$, three-coordinated O on $Cu_2O(110)$, and two-coordinated O on $Cu_2O(100)$ were identified as the catalytically active sites for the production of acrolein, propylene oxide, and CO_2, respectively. These results reveal that crystal-plane engineering of oxide catalysts could be a useful strategy for developing selective catalysts and for gaining fundamental understanding of complex heterogeneous catalytic reactions at the molecular level.*

Propylene oxide (PO) and acrolein rank among the top industrial chemical intermediates produced annually and are currently manufactured by the partial oxidation of propylene. The selective catalytic partial oxidation of propylene with O_2 is the desirable green method for their industrial production. This method has been realized for the industrial production of acrolein with bismuth/molybdenum-based mixed-oxide catalysts; however, the current major methods for the industrial production of propylene oxide are the environmentally unfriendly chlorohydrin process and equally environmentally unfriendly variations of the Halcon process.[1] Thus, great effort has been devoted to the development of efficient catalysts for propylene epoxidation with O_2,[2–5] for which promising active components are limited to the IB elements (Cu, Ag, and Au). Copper is much more economical than gold and silver for use as an industrial catalyst. Copper-based catalysts have been examined for the partial oxidation of propylene with O_2,[5] and cuprous oxide, instead of metallic Cu, has been proposed as the active structure.[6] The morphology of the oxide nanoparticle determines the exposed crystal planes and the surface composition/structure and thus significantly influences its catalytic performance.[7] Recently, uniform Cu_2O nanocrystals with different morphologies were synthesized and demonstrated to exhibit morphology-dependent catalytic activity in CO oxidation with excess or stoichiometric O_2,[8] the photocatalytic degradation of dyes,[9] and liquid-phase organic reactions.[10] Herein we report that the morphology and exposed crystal planes of capping-ligand-free Cu_2O nanocrystals control the catalytic selectivity as well as the catalytic activity in propylene oxidation with O_2; we also reveal the underlying structure–activity relationships of this complex heterogeneous catalytic reaction at the molecular level and identify the catalytically active sites (Scheme 1).

Uniform cubic, octahedral, and rhombic-dodecahedral Cu_2O nanocrystals were synthesized according to well-established procedures, in which poly(*N*-vinyl-2-pyrrolidone) (PVP) and oleic acid (OA) capping ligands were employed to prepare octahedral and rhombic-dodecahedral Cu_2O nanocrystals, respectively, whereas no capping ligand was used for cubic Cu_2O nanocrystals.[11] As-synthesized cubic Cu_2O nanocrystals (denoted as c-Cu_2O) have sizes between 400 and

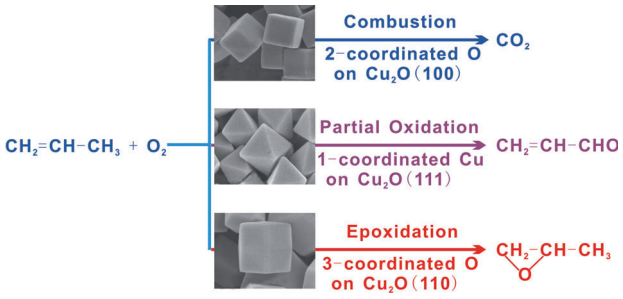

Scheme 1. Crystal-plane-controlled selectivity of Cu_2O catalysts in the oxidation of propylene with molecular oxygen. The catalytically active sites on Cu_2O are indicated for the different reaction pathways.

[*] Q. Hua,[+] T. Cao,[+] Dr. Z. Jiang, L. Luo, Prof. Dr. W. Huang
Hefei National Laboratory for Physical Sciences at the Microscale, Collaborative Innovation Center of Suzhou Nano Science and Technology, CAS Key Laboratory of Materials for Energy Conversion, Department of Chemical Physics
University of Science and Technology of China
Jinzhai Road 96, Hefei 230026 (China)
E-mail: huangwx@ustc.edu.cn
Dr. X.-K. Gu,[+] Prof. Dr. W.-X. Li
State Key Laboratory of Catalysis
Dalian Institute of Chemical Physics, Chinese Academy of Sciences
Zhongshan Road 457, Dalian 116023 (China)
Prof. Dr. J. Lu,[+] X. Pan
Institute of Physical Chemistry, Zhejiang Normal University
Jinhua 321004 (China)
[+] These authors contributed equally.

[**] This research was financially supported by the National Natural Science Foundation of China (21173204, 11079033, 21225315), the National Basic Research Program of China (2013CB933104, 2010CB923301), and the Strategic Priority Research Program of the Chinese Academy of Sciences (XDA09030103).
Supporting information for this article is available on the WWW under http://dx.doi.org/10.1002/anie.201402374.

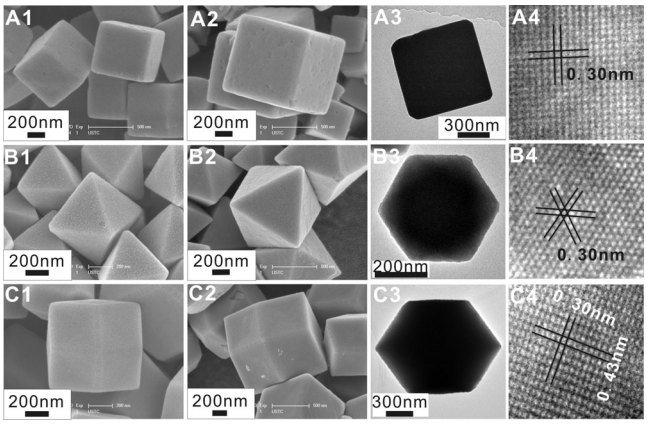

Figure 1. A1) SEM image of as-synthesized Cu_2O cubes; A2–A4) SEM, TEM, and HRTEM images of as-synthesized Cu_2O cubes subjected to controlled treatment at 200 °C for 0.5 h; B1) SEM image of as-synthesized Cu_2O octahedra capped with PVP; B2–B4) SEM, TEM, and HRTEM images of capping-ligand-free Cu_2O octahedra; C1) SEM image of as-synthesized Cu_2O rhombic dodecahedra capped with OA; C2–C4) SEM, TEM, and HRTEM images of capping-ligand-free Cu_2O rhombic dodecahedra. The distances 0.43 and 0.30 nm correspond to the {001} and {110} planes of Cu_2O, respectively.

700 nm and selectively expose six {100} crystal planes (Figure 1 A1; see also Figure S1 A in the Supporting Information). As-synthesized octahedral Cu_2O nanocrystals (denoted as o-Cu_2O-PVP) have sizes between 300 and 600 nm and selectively expose eight {111} crystal planes (Figure 1 B1; see also Figure S2 A). As-synthesized rhombic-dodecahedral Cu_2O nanocrystals (denoted as d-Cu_2O-OA) have sizes between 600 and 900 nm and selectively expose 12 {110} crystal planes (Figure 1 C1; see also Figure S3 A). XRD (see Figure S4) and Cu 2p XPS (Figure 2 A) confirmed that their crystal phases had the Cu_2O structure and their surfaces remained as Cu_2O. The specific BET surface areas of c-Cu_2O, o-Cu_2O-PVP, and d-Cu_2O-OA were measured to be 1.49, 1.74, and 0.774 $m^2 g^{-1}$, respectively (see Figure S5). Because of the synthetic procedures used, o-Cu_2O-PVP and d-Cu_2O-OA are capped (with PVP and OA, respectively), but c-Cu_2O is not. As shown in Figure 2 B–D, whereas o-Cu_2O-PVP exhibits N 1s and C 1s XPS features and C–H stretching-vibration bands arising from capped PVP, and d-Cu_2O-OA exhibits C 1s XPS features and C–H stretching-vibration bands arising from capped OA, c-Cu_2O only exhibits C 1s features corresponding to adventitious carbon (284.8 eV) and carbonate species (288.3 eV)[12] but no C–H stretching-vibration bands.

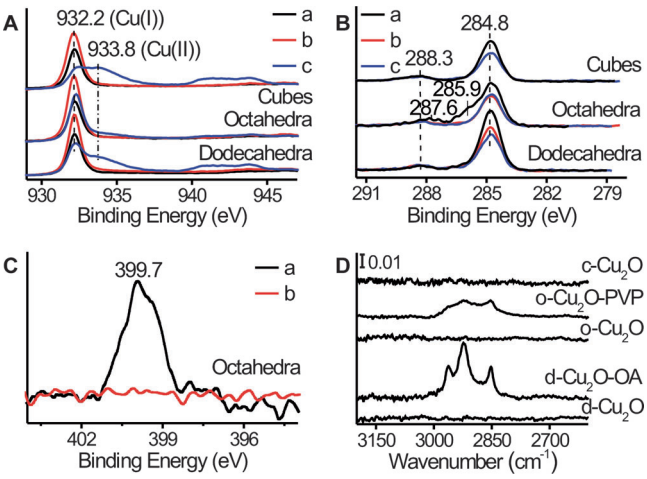

Figure 2. A) Cu $2p_{3/2}$, B) C 1s, and C) N 1s XPS spectra, and D) infrared spectra of a) as-synthesized Cu_2O nanocrystals, b) capping-ligand-free Cu_2O nanocrystals, and c) capping-ligand-free Cu_2O nanocrystals after evaluation of the catalytic performance up to 250 °C.

The removal of capping ligands on nanocrystals without a change in their composition and structure remains challenging, but is essential for their use as catalysts.[13] We found that the controlled treatment of o-Cu_2O-PVP and d-Cu_2O-OA in a stream of a C_3H_6/O_2 mixture balanced with N_2 ($C_3H_6/O_2/N_2$ 2:1:22) enabled the selective removal of capping ligands without changing the composition and structure of the nanocrystals. Upon the controlled treatment of o-Cu_2O-PVP in this way at 200 °C for 0.5 h, the N 1s peak disappeared (Figure 2 C), the C 1s peaks at 285.9 and 287.6 eV also disappeared, and the C 1s peak at 284.8 eV was greatly attenuated (Figure 2 B); furthermore, the C–H vibration bands in the infrared spectrum disappeared (Figure 2 D). In the case of d-Cu_2O-OA, the treatment temperature was increased to 215 °C to remove the oleic acid surfactant, as evidenced by the disappearance of the C–H vibration bands in the infrared spectrum after treatment for 0.5 h (Figure 2 D) and the great attenuation of the C 1s peak at 284.8 eV (Figure 2 B). The morphology, bulk structure, and surface composition of o-Cu_2O-PVP (Figure 1 B2–B4, Figure 2 A; see also Figure S4) and d-Cu_2O-OA (Figure 1 C2–C4, Figure 2 A; see also Figure S4) did not change during this controlled treatment. Thus, we successfully acquired capping-ligand-free uniform octahedral (denoted as o-Cu_2O) and rhombic-dodecahedral (denoted as d-Cu_2O) Cu_2O nanocrystals. Their synthesis was further supported by the experimental observations that CO was clearly chemisorbed on o-Cu_2O and d-Cu_2O, but not on o-Cu_2O-PVP and d-Cu_2O-OA (see Figure S6). C 1s XPS results (Figure 2 B) demonstrated that the surface carbon species on o-Cu_2O and d-Cu_2O as well as c-Cu_2O were carbonate and adventitious carbon. Both are common on oxide-catalyst surfaces.

The novelty of our method to remove capping ligands on Cu_2O nanocrystals is the use of an atmosphere consisting of both oxidizing gas (O_2) and reducing gas (C_3H_6) with appropriate concentrations. On one hand, capping ligands on Cu_2O nanocrystals could be adequately oxidized by O_2 and removed at relatively low temperatures to avoid a high-temperature-induced morphology change; on the other hand, the coexistence of C_3H_6 and O_2 in the atmosphere could cooperatively prevent Cu_2O nanocrystals from both oxidation and reduction. The latter hypothesis is further supported by the experimental results that the morphology, bulk structure, and surface composition of as-synthesized capping-ligand-free c-Cu_2O remained unchanged after controlled oxidative treatment at 200 °C for 0.5 h (Figure 1 A2–A4, Figure 2 A; see also Figure S4). Our method provides a promising general strategy for the selective removal of chemisorbed capping ligands on catalytic nanocrystals without changing their composition and structure.

The catalytic performance of the Cu_2O nanocrystals in propylene oxidation with O_2 was evaluated. Propylene oxide, acrolein, and carbon dioxide were identified as the dominant reaction products. o-Cu_2O and d-Cu_2O were more catalytically active than the corresponding nanocrystals o-Cu_2O-PVP and d-Cu_2O-OA (see Figure S7), thus demonstrating that capping ligands on as-synthesized Cu_2O nanocrystals suppress their catalytic activity. Capping-ligand-free Cu_2O nanocrystals exhibited distinct morphology-dependent catalytic activity (Figure 3 A–C). All Cu_2O nanocrystals became active at

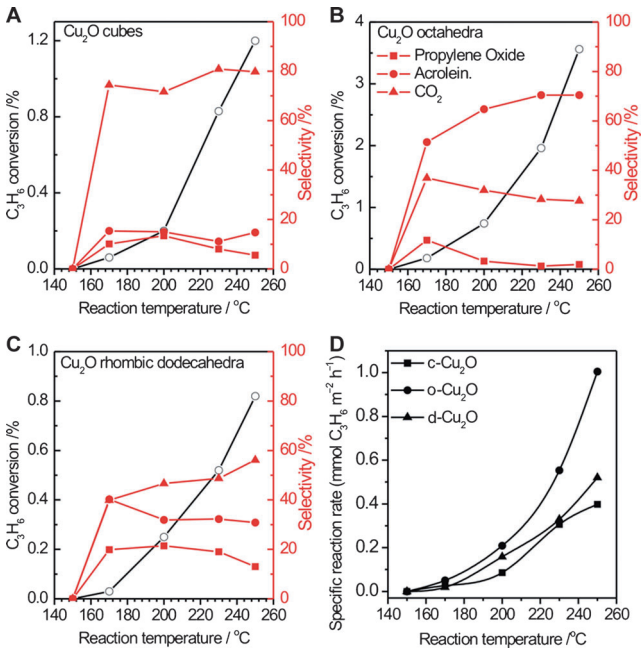

Figure 3. C_3H_6 conversion and selectivity for propylene oxide, acrolein, and CO_2 of the C_3H_6 oxidation with O_2 as catalyzed by capping-ligand-free A) Cu_2O cubes, B) octahedra, and C) rhombic dodecahedra. D) Specific reaction rate of C_3H_6 oxidation with molecular oxygen as catalyzed by capping-ligand-free Cu_2O cubes (c-Cu_2O), octahedra (o-Cu_2O), and rhombic dodecahedra (d-Cu_2O).

170 °C, and C_3H_6 conversion increased with the reaction temperature. At the same temperature, C_3H_6 conversion was catalyzed by the Cu_2O nanocrystals with varying degrees of efficiency according to the order o-Cu_2O > c-Cu_2O > d-Cu_2O. The specific propylene reaction rate normalized to the specific surface area of various Cu_2O nanocrystals (Figure 3 D) also followed the order o-Cu_2O > d-Cu_2O > c-Cu_2O. Thus, Cu_2O octahedra are more active in catalyzing C_3H_6 oxidation with O_2 than Cu_2O cubes and rhombic dodecahedra. This behavior exemplifies well the recently established concept of the morphology-controlled catalytic activity of oxide catalysts.[7]

Very interestingly, we observed that the catalytic selectivity of Cu_2O nanocrystals in propylene oxidation with O_2 also depended sensitively on their morphology. c-Cu_2O was very selective in catalyzing the propylene combustion reaction with a CO_2 selectivity of around 80% under the investigated reaction temperatures (Figure 3 A), whereas o-Cu_2O exhibited the highest selectivity for the partial oxidation of propylene to acrolein (Figure 3 B). At 170 °C, the selectivity for the formation of acrolein, propylene oxide, and CO_2 was 51, 12, and 37%, respectively. As the reaction temperature was increased, the selectivity for acrolein continued to increase at the expense of the selectivity for propylene oxide and CO_2, and the selectivity for acrolein reached 71% at 250 °C. d-Cu_2O exhibited comparable selectivity for the formation of propylene oxide (20%), acrolein (40%), and CO_2 (40%) at 170 °C (Figure 3 C). When the reaction temperature was increased to 250 °C, the selectivity for propylene oxide did not change initially, but then decreased to 13% at 250 °C; the selectivity for acrolein gradually decreased; and the selectivity for CO_2 gradually increased. Therefore, in the catalysis of propylene oxidation with O_2, c-Cu_2O is the most selective of the three nanocrystal catalysts for the combustion of propylene to produce CO_2, o-Cu_2O is the most selective for the partial oxidation of propylene to produce acrolein, and d-Cu_2O is the most selective for the epoxidation of propylene to produce propylene epoxide. These results for the first time demonstrate that the selectivity of oxide catalysts in reactions as complex as propylene oxidation with O_2 can be tuned by changing their morphology, thus offering a novel strategy to control the selectivity of oxide catalysts.

Propylene epoxidation with molecular O_2 is a highly desirable reaction but remains very challenging. We calculated the formation rate of propylene oxide and the turnover frequency (TOF) on the basis of surface Cu atoms for propylene oxidation with O_2 as catalyzed by d-Cu_2O at 250 °C and compared both values with those found for the reaction catalyzed by previously reported representative supported copper-based catalysts (see Table S1 in the Supporting Information). Owing to the very small specific surface area of d-Cu_2O, the formation rate of propylene oxide (0.057 mmol $g_{catalyst}^{-1}$ h^{-1}) was quite low; however, the TOF value reached 1.46×10^{-3} s^{-1} and is comparable to that of the most active K^+-promoted highly dispersed supported CuO_x catalysts at 350 °C.[5b] For d-Cu_2O nanocrystal catalysts, there is plenty of room to increase the propylene conversion rate by reducing their size and enlarging their specific surface area. Thus, Cu_2O rhombic dodecahedra are a promising catalyst for propylene oxidation with O_2 to selectively produce propylene oxide together with acrolein.

Following the evaluation of the catalytic performance of the nanocatalysts up to 250 °C, SEM and TEM results showed that c-Cu_2O, o-Cu_2O, and d-Cu_2O maintained their original morphologies and phase structure well (see Figures S1 A3, S2 A3, S3 A3, and S4), but features arising from CuO appeared in the Cu $2p_{3/2}$ XPS spectra (Figure 2 A). This observation indicates the partial oxidation of Cu_2O nanocrystals during the catalytic reaction; however, high-resolution TEM images (see Figure S1 D3, S2 D3, and S3 D3) failed to show any lattice fringes arising from CuO. This result implies the likely formation of very thin CuO islands on the surface of Cu_2O nanocrystals. No obvious accumulation of adventitious carbon and carbonate were observed by C 1s XPS (Figure 2 B). We also investigated the stability of o-Cu_2O at 240 °C (see Figure S8 A) and d-Cu_2O at 215 °C in the catalysis of propylene oxidation with O_2 (see Figure S8 B). o-

Cu_2O was very stable at 240 °C and promoted approximately 2.5% C_3H_6 conversion with around 80% selectivity for the formation of acrolein. d-Cu_2O was not stable even at 215 °C. During the reaction, C_3H_6 conversion slowly decreased from 0.35 to 0.15%, the selectivity for propylene oxide slowly decreased from 18.4 to 12%, and the selectivity for acrolein slowly increased from 33.4 to 45.6%. After the stability test, the surface of o-Cu_2O was slightly oxidized, but that of d-Cu_2O was seriously oxidized (see Figure S9).

The above results clearly reveal that the morphology of oxide nanocrystals controls their catalytic selectivity as well as their catalytic activity. Figure 4 compares the DRIFTS spectra acquired for the chemisorption of C_3H_6 and $C_3H_6+O_2$ on

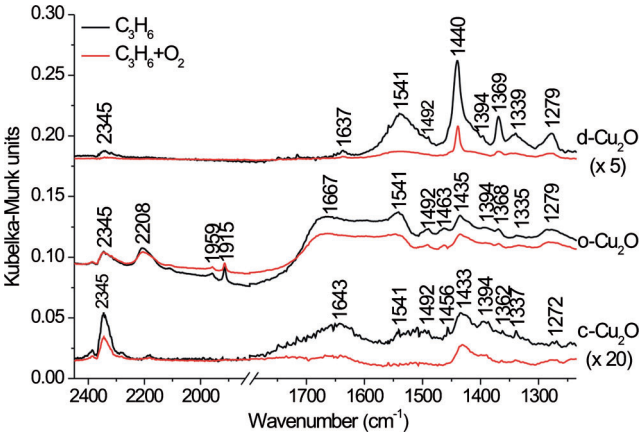

Figure 4. DRIFTS spectra of C_3H_6 and $C_3H_6+O_2$ chemisorption on capping-ligand-free Cu_2O cubes (c-Cu_2O), octahedra (o-Cu_2O), and rhombic dodecahedra (d-Cu_2O) at 230 °C. DRIFTS = diffuse reflectance infrared Fourier transform spectroscopy.

different Cu_2O nanocrystals at 230 °C. The first observation is that on each type of Cu_2O nanocrystal, the vibrational features of $C_3H_6+O_2$ chemisorption are similar to those of C_3H_6 chemisorption, except that their intensities are reduced. This observation infers that propylene oxidation with O_2 as catalyzed by Cu_2O follows the Mars–van Krevelen (MvK) mechanism, and the lattice oxygen atoms of the Cu_2O surface are the active oxygen species. The second observation is that o-Cu_2O exhibits substantially stronger vibrational features than those of c-Cu_2O and d-Cu_2O. Thus, o-Cu_2O is most active toward the chemisorption and surface reaction of C_3H_6, in agreement with the experimental result that o-Cu_2O is much more catalytically active than c-Cu_2O and d-Cu_2O. The third observation is that the vibrational features vary on different Cu_2O nanocrystals and indicates the morphology-dependent formation of surface adsorbates/intermediates upon C_3H_6 oxidation on Cu_2O nanocrystals. This behavior corresponds well to the morphology-dependent catalytic selectivity of the nanocrystals in propylene oxidation with O_2.

To assist the assignment of the observed vibrational bands (see Table S2), we measured DRIFTS spectra for C_3D_6 chemisorption (see Figure S10) and CO_2 chemisorption (see Figure S11) on different Cu_2O nanocrystals. o-Cu_2O, c-Cu_2O, and d-Cu_2O expose {111}, {100}, and {110} crystal planes, respectively, whose surface structures were optimized (see Figure S12).[11] Coordinatively saturated Cu (Cu_{CSA}) and O (O_{CSA}) in the bulk cubic Cu_2O are two-coordinated and four-coordinated, respectively. The $Cu_2O(111)$ surface is terminated with three-coordinated O_{CUS} (CUS = coordinatively unsaturated) in the top layer and one-coordinated Cu (Cu_{CUS}) and Cu_{CSA} in the second layer in a 1:3 ratio. The $Cu_2O(100)$ surface is terminated with two-coordinated O atoms (O_{CUS}) in the top layer and Cu_{CSA} in the second layer. The $Cu_2O(110)$ surface is terminated with three-coordinated O_{CUS} and Cu_{CSA} in the top layer and Cu_{CSA} in the second layer. Therefore, C_3H_6 adsorption on $Cu_2O(111)$, (100), and (110) surfaces was also studied by DFT calculations, the results of which (Figure 5) support the experimental observations well. On $Cu_2O(111)$, C_3H_6 is preferentially adsorbed at the Cu_{CUS} site to form Cu_{CUS}–C_3H_6(a) with an adsorption energy of −1.53 eV and a C=C stretching frequency of 1560 cm^{-1}. Experimentally, on the o-Cu_2O surface, chemisorbed C_3H_6

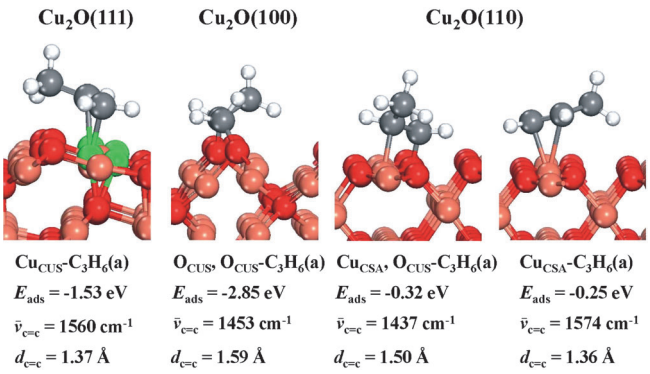

Figure 5. Optimized structures of the most stable C_3H_6(a) species on $Cu_2O(111)$, (100), and (110) surfaces with the adsorption energy, C=C stretching frequency, and C=C bond length. Red, gray, white, pink, and green balls represent O, C, H, coordinatively saturated Cu, and coordinatively unsaturated Cu, respectively.

species are only C_3H_6(a) with a C=C stretching frequency of 1541 cm^{-1}. On $Cu_2O(100)$, C_3H_6 preferentially bonds to two neighboring two-coordinated O_{CUS} sites to form O_{CUS},O_{CUS}–C_3H_6(a) with an adsorption energy of −2.85 eV and a C=C stretching frequency of 1453 cm^{-1}. Experimentally, on the c-Cu_2O surface, the dominant chemisorbed C_3H_6 species exhibits a C=C stretching frequency of 1428 cm^{-1}. On Cu_2O-(110), bridge-adsorbed Cu_{CSA},O_{CUS}–C_3H_6(a) ($\bar{\nu}_{C=C}$ = 1437 cm^{-1}) and atop-adsorbed Cu_{CSA}–C_3H_6(a) ($\bar{\nu}_{C=C}$ = 1574 cm^{-1}) have similar adsorption energies. Experimentally, on the d-Cu_2O surface, C_3H_6(a) species with C=C stretching-vibration frequencies of 1541 and 1428 cm^{-1} were both observed. The $\bar{\nu}_{C=C}$ bands of O_{CUS},O_{CUS}–C_3H_6(a) and Cu_{CSA},O_{CUS}–C_3H_6(a) at 1428 cm^{-1} are indistinguishable from the C–H bending-vibration bands (Figure 4), but their presence is evidenced in the case of C_3D_6 chemisorption (see Figure S10), in which case the C–D bending-vibration bands are red-shifted away from the $\bar{\nu}_{C=C}$ bands.

Besides the different chemisorbed C_3H_6(a) species, different surface intermediates form on various Cu_2O nanocrystals. On the o-Cu_2O surface, chemisorbed acrolein ($\bar{\nu}_{C=O}$ at 1667 cm^{-1}) is evident, and chemisorbed allyl ($\bar{\nu}_{C-C-C}$ at 1428

and 1406 cm^{-1}; see Figure S10) and allene species ($\tilde{\nu}_{C=C=C}$ at 1959 and 1915 cm^{-1}), which are key intermediates for the partial oxidation of propylene to acrolein,[14] are also present. These observations agree with the high selectivity of o-Cu_2O nanocrystals in catalyzing the partial oxidation of propylene to acrolein and indicate Cu_{CUS}–C_3H_6(a) on Cu_2O(111) as the active species. The C=C bond distance of Cu_{CUS}–C_3H_6(a) was calculated to be 1.37 Å, whereas that of the gas-phase C_3H_6 molecule is 1.34 Å. Thus, the C=C bond of Cu_{CUS}–C_3H_6(a) is only marginally activated, and its entity can reasonably be preserved in the subsequent surface reactions, thus leading to the formation of acrolein.

On the c-Cu_2O surface, CO_2(a) ($\tilde{\nu}_{as}(CO_2)$ at 2345 cm^{-1}) and carbonate/carboxylate species (broad bands between 1650 and 1350 cm^{-1}) are dominant surface intermediates, in agreement with the high selectivity of c-Cu_2O in catalyzing propylene combustion. The C=C bond distance of O_{CUS},O_{CUS}–C_3H_6(a) on Cu_2O(100) was calculated to be 1.59 Å; thus, its C=C bond is significantly weakened and should undergo facile cleavage in the subsequent surface reactions. The epoxidation and combustion of propylene are the reaction pathways involving cleavage of the C=C bond. DFT calculation results (see Figure S13 A) show that the activation energy for the epoxidation of O_{CUS},O_{CUS}–C_3H_6(a) to give chemisorbed propylene oxide (C_3H_6O(a)) and the decomposition of O_{CUS},O_{CUS}–C_3H_6(a) into adsorbed CH_2(a) and $CHCH_3$(a) is 2.09 and 1.02 eV, respectively. This result indicates that O_{CUS},O_{CUS}–C_3H_6(a) should preferentially undergo the combustion reaction, thus supporting the experimental results for c-Cu_2O.

On the d-Cu_2O surface, a chemisorbed allyl species is present (see Figure S10), and the presence of C_3H_6O(a) is indicated by the strong and narrow C–H bending-vibration band at 1440 cm^{-1}. Such a feature does not appear in the case of C_3H_6 chemisorption on c-Cu_2O and o-Cu_2O and can be reasonably assigned to $\delta(CH_2)$ of C_3H_6O(a) by comparison with the infrared spectra of propylene, acrolein, and propylene oxide.[15] These observations agree with the production of both acrolein and propylene oxide through propylene oxidation with O_2 as catalyzed by d-Cu_2O. The C=C bond distance of Cu_{CSA}–C_3H_6(a) on Cu_2O(110) was calculated to be 1.36 Å, and thus Cu_{CSA}–C_3H_6(a) is reasonably considered to be the active species for the formation of acrolein; Cu_{CSA},O_{CUS}–C_3H_6(a) on Cu_2O(110) exhibits a significantly weakened C=C bond with a C=C bond distance of 1.50 Å and can reasonably be expected to undergo the surface reactions involving the breaking of the C=C bond. Interestingly, the results of DFT calculations (see Figure S13 B) show that the activation energy for the epoxidation of Cu_{CSA},O_{CUS}–C_3H_6(a) to give C_3H_6O(a) and the decomposition of Cu_{CSA},O_{CUS}-C_3H_6(a) into adsorbed CH_2(a) and $CHCH_3$(a) is 1.28 and 2.08 eV, respectively. These activation energies indicate that Cu_{CSA},O_{CUS}–C_3H_6(a) should preferentially undergo the epoxidation reaction, thus supporting the experimental results for d-Cu_2O. The different reactivities of O_{CUS},O_{CUS}–C_3H_6(a) on Cu_2O(100) and Cu_{CSA},O_{CUS}–C_3H_6(a) on Cu_2O(110) reflect the different reactivities of two-coordinated O_{CUS} on Cu_2O(100) and three-coordinated O_{CUS} on Cu_2O(110). Two-coordinated O_{CUS} is more electrophilic than three-coordinated O_{CUS} and is thus more able to completely break the C=C bond of propylene to result in the combustion reaction. These results provide unprecedented comprehensive fundamental understanding of the structure–activity relationships and active sites of Cu_2O catalysts in the catalysis of propylene oxidation with O_2 (Scheme 1).

In summary, we have successfully revealed the crystal-plane-controlled selectivity of Cu_2O catalysts in the catalysis of propylene oxidation with O_2 and gained an understanding of their structure–activity relationships and catalytically active sites by the use of capping-ligand-free Cu_2O octahedra, cubes, and rhombic dodecahedra as catalysts. Cu_2O octahedra enclosed by {111} crystal planes are most selective for the formation of acrolein, and one-coordinated Cu^I on Cu_2O(111) is the active site; Cu_2O cubes enclosed by {100} crystal planes are most selective for the formation of CO_2, and two-coordinated O on Cu_2O(100) is the active site; and Cu_2O rhombic dodecahedra enclosed by {110} crystal planes are most selective for the formation of propylene oxide, and three-coordinated O on Cu_2O(110) is the active site. These results reveal a strategy based on the morphology (crystal-plane) engineering of oxide catalysts as an effective approach for both the discovery of selective catalysts and the broadening of our fundamental understanding of heterogeneous catalysis. On one hand, 100% selectivity for the targeted product is the ultimate goal of heterogeneous catalysis. A catalyst nanoparticle enclosed by different crystal planes is intrinsically inappropriate as a means to reach this ultimate goal because different crystal planes will exhibit various selectivities. In this regard, catalyst nanocrystals that have a uniform morphology and selectively expose a single type of crystal plane are promising as highly selective catalysts. On the other hand, fundamental understanding of structure–activity relationships and active sites is a long-standing challenge for complex heterogeneous catalytic reactions. The traditional approach is to study single-crystal-based model catalysts under ultrahigh-vacuum conditions, but these systems often suffer from the so-called "pressure gap" and "materials gap". Catalyst nanocrystals with uniform morphologies and well-defined structures are appropriate model catalysts for fundamental studies of practical heterogeneous catalytic reactions. The acquired fundamental understanding will be invaluable for the design of efficient catalysts. The success of this approach can be anticipated from our present results, which show that Cu_2O octahedra are a promising catalyst for propylene oxidation with O_2 to produce acrolein, and that uniform Cu_2O particles that selectively expose a high density of three-coordinated O sites are active in catalyzing propylene epoxidation with O_2 to produce propylene oxide: a highly desirable but very challenging catalytic reaction.

Received: February 13, 2014
Published online: April 1, 2014

Keywords: active sites · nanocatalysis · oxide catalysts · reaction mechanisms · surface chemistry

[1] *Handbook of Heterogeneous Catalysis*, *Vol. 5* (Eds.: G. Ertl, H. Knözinger, J. Weitkamp), VCH, Weinheim, **1997**.

[2] a) T. A. Nijhuis, M. Makkee, J. A. Moulijn, B. M. Weckhuysen, *Ind. Eng. Chem. Res.* **2006**, *45*, 3447 – 3459; b) F. Cavani, J. H. Teles, *ChemSusChem* **2009**, *2*, 508 – 534.

[3] a) T. Hayashi, K. Tanaka, M. Haruta, *J. Catal.* **1998**, *178*, 566 – 575; b) B. Chowdhury, J. J. Bravo-Suárez, M. Daté, S. Tsubota, M. Haruta, *Angew. Chem.* **2006**, *118*, 426 – 429; *Angew. Chem. Int. Ed.* **2006**, *45*, 412 – 415; c) S. Lee, L. M. Molina, M. J. López, J. A. Alonso, B. Hammer, B. Lee, S. Seifert, R. E. Winans, J. W. Elam, M. J. Pellin, S. Vajda, *Angew. Chem.* **2009**, *121*, 1495 – 1499; *Angew. Chem. Int. Ed.* **2009**, *48*, 1467 – 1471; d) J. Huang, T. Akita, J. Faye, T. Fujitani, T. Takei, M. Haruta, *Angew. Chem.* **2009**, *121*, 8002 – 8006; *Angew. Chem. Int. Ed.* **2009**, *48*, 7862 – 7866.

[4] a) F. W. Zemichael, A. Palermo, M. Tikhov, R. M. Lambert, *Catal. Lett.* **2002**, *80*, 93 – 98; b) M. Luo, J. Lu, C. Li, *Catal. Lett.* **2003**, *86*, 43 – 49; c) J. Lu, J. J. Bravo-Suárez, A. Takahashi, M. Haruta, S. T. Oyama, *J. Catal.* **2005**, *232*, 85 – 95; d) Y. Lei, F. Mehmood, S. Lee, J. Greeley, B. Lee, S. Seifert, R. E. Winans, J. W. Elam, R. J. Meyer, P. C. Redfern, D. Teschner, R. Schlögl, M. J. Pellin, L. A. Curtiss, S. Vajda, *Science* **2010**, *328*, 224 – 228; e) L. M. Molina, S. Lee, K. Sell, G. Barcaro, A. Fortunelli, B. Lee, S. Seifert, R. E. Winans, J. W. Elam, M. J. Pellin, I. Barke, V. von Oeynhausen, Y. Lei, R. J. Meyer, J. A. Alonso, A. F. Rodríguez, A. Kleibert, S. Giorgio, C. R. Henry, K.-H. Meiwes-Broer, S. Vajda, *Catal. Today* **2011**, *160*, 116 – 130.

[5] a) O. P. H. Vaughan, G. Kyriakou, N. Macleod, M. Tikhov, R. M. Lambert, *J. Catal.* **2005**, *236*, 401 – 404; b) H. Chu, L. Yang, Q. Zhang, Y. Wang, *J. Catal.* **2006**, *241*, 225 – 228; c) W. Su, S. Wang, P. Ying, Z. Feng, C. Li, *J. Catal.* **2009**, *268*, 165 – 174; d) L. Yang, J. He, Q. Zhang, Y. Wang, *J. Catal.* **2010**, *276*, 76 – 84; e) A. Marimuthu, J. Zhang, S. Linic, *Science* **2013**, *339*, 1590 – 1593; f) R. K. Grasselli, J. D. Burrington, *Adv. Catal.* **1981**, *30*, 133 – 163; g) D. Torres, N. Lopez, F. Illas, R. M. Lambert, *Angew. Chem.* **2007**, *119*, 2101 – 2104; *Angew. Chem. Int. Ed.* **2007**, *46*, 2055 – 2058.

[6] a) G. W. Keulks, L. D. Krenske, T. M. Notermann, *Adv. Catal.* **1979**, *27*, 183 – 225; b) K. H. Schulz, D. F. Cox, *Surf. Sci.* **1992**, *262*, 318 – 334; c) K. H. Schulz, D. F. Cox, *J. Catal.* **1993**, *143*, 464 – 480; d) J. B. Reitz, E. I. Solomon, *J. Am. Chem. Soc.* **1998**, *120*, 11467 – 11478; e) W. Zhu, Q. Zhang, Y. Wang, *J. Phys. Chem. C* **2008**, *112*, 7731 – 7734; f) J. He, Q. Zhai, Q. Zhang, W. Deng, Y. Wang, *J. Catal.* **2013**, *299*, 53 – 66.

[7] a) J. A. van Bokhoven, *ChemCatChem* **2009**, *1*, 363 – 364; b) K. B. Zhou, Y. D. Li, *Angew. Chem.* **2012**, *124*, 622 – 635; *Angew. Chem. Int. Ed.* **2012**, *51*, 602 – 613; c) W. X. Huang, *Top. Catal.* **2013**, *56*, 1363 – 1376.

[8] a) H. Bao, W. Zhang, Q. Hua, Z. Jiang, J. Yang, W. X. Huang, *Angew. Chem.* **2011**, *123*, 12502 – 12506; *Angew. Chem. Int. Ed.* **2011**, *50*, 12294 – 12298; b) Q. Hua, T. Cao, H. Bao, Z. Jiang, W. X. Huang, *ChemSusChem* **2013**, *6*, 1966 – 1972.

[9] a) W.-C. Huang, L.-M. Lyu, Y.-C. Yang, M. H. Huang, *J. Am. Chem. Soc.* **2012**, *134*, 1261 – 1267; b) Y. Zhang, B. Deng, T. Zhang, D. Gao, A. Xu, *J. Phys. Chem. C* **2010**, *114*, 5073 – 5079; c) J.-Y. Ho, M. H. Huang, *J. Phys. Chem. C* **2009**, *113*, 14159 – 14164.

[10] a) Y. Xu, H. Wang, Y. Yu, L. Tian, W. Zhao, B. Zhang, *J. Phys. Chem. C* **2011**, *115*, 15288 – 15296; b) L. Li, C. Nan, Q. Peng, Y. Li, *Chem. Eur. J.* **2012**, *18*, 10491 – 10496; c) K. Chanda, S. Rej, M. H. Huang, *Chem. Eur. J.* **2013**, *19*, 16036 – 16043.

[11] a) H. Z. Bao, W. H. Zhang, D. L. Shang, Q. Hua, Y. S. Ma, Z. Q. Jiang, J. L. Yang, W. X. Huang, *J. Phys. Chem. C* **2010**, *114*, 6676 – 6680; b) Q. Hua, D. Shang, W. Zhang, K. Chen, S. Chang, Y. Ma, Z. Jiang, J. Yang, W. X. Huang, *Langmuir* **2011**, *27*, 665 – 671.

[12] T. F. Moulder, W. J. Stickle, P. E. Sobol, K. D. Bomben, *Handbook of X-ray Photoelectron Spectroscopy*, PerkinElmer, Eden Prairie, MN, **1992**.

[13] J. A. Lopez-Sanchez, N. Dimitratos, C. Hammond, G. L. Brett, L. Kesavan, S. White, P. Miedziak, R. Tiruvalam, R. L. Jenkins, A. F. Carley, D. Knight, C. J. Kiely, G. J. Hutchings, *Nat. Chem.* **2011**, *3*, 551 – 556.

[14] C. Zhao, I. E. Wachs, *J. Phys. Chem. C* **2008**, *112*, 11363 – 11372.

[15] http://webbook.nist.gov/cgi/cbook.cgi?ID = C115071&Units = SI&Type = IR-SPEC&Index = 1#IR-SPEC (IR spectrum of propylene); http://webbook.nist.gov/cgi/cbook.cgi?ID = C107028&Units = SI&Type = IR-SPEC&Index = 1#IR-SPEC (IR spectrum of acrolein); http://webbook.nist.gov/cgi/cbook.cgi?ID = C75569&Units = SI&Type = IR-SPEC&Index = 1#IR-SPEC (IR spectrum of propylene oxide).

